ACS ENGINEERING Au
AN OPEN ACCESS JOURNAL OF THE AMERICAN CHEMICAL SOCIETY

pubs.acs.org/engineeringau

Article

New Perspectives into Cellulose Fast Pyrolysis Kinetics Using a Py-GC × GC-FID/MS System

Gorugantu SriBala, Diana C. Vargas, Pavlo Kostetskyy, Ruben Van de Vijver, Linda J. Broadbelt, Guy B. Marin, and Kevin M. Van Geem*

Cite This: *ACS Eng. Au* 2022, 2, 320−332

Read Online

ACCESS | Metrics & More | Article Recommendations | Supporting Information

ABSTRACT: Cellulose pyrolysis is reportedly influenced by factors such as sample size, crystallinity, or different morphologies. However, there seems to be a lack of understanding of the mechanistic details that explain the observed differences in the pyrolysis yields. This study aims to investigate the influence of particle size and crystallinity of cellulose by performing pyrolysis reactions at temperatures of 673−873 K using a micropyrolyzer apparatus coupled to a GC × GC-FID/TOF-MS and a customized GC-TCD. Over 60 product species have been identified and quantified for the first time, including water. Crystalline cellulose with an average particle size of 30−50 × 10^{-6} m produced 50−60 wt % levoglucosan. Predominantly amorphous cellulose with an average particle size of 10−20 × 10^{-6} m resulted in remarkably low yields (10−15 wt %) of levoglucosan complemented by higher yields of water and glycolaldehyde. A detailed kinetic model for cellulose pyrolysis was used to obtain mechanistic insights into the different pyrolysis product compositions. The kinetics of the mid-chain dehydration and fragmentation reactions strongly influence the total yields of low-molecular weight products (LMWPs) and are affected by cellulose chain arrangement. Levoglucosan yields are very sensitive to the activation of parallel cellulose decomposition reactions. This can be attributed to the mid-chain reactions forming smaller chains with the levoglucosan ends, which remain in the solid phase and react further to form LMWPs. Direct quantification of water helped to improve the description of the dehydration, giving further indications of the dominant role of mid-chain reaction pathways in amorphous cellulose pyrolysis.

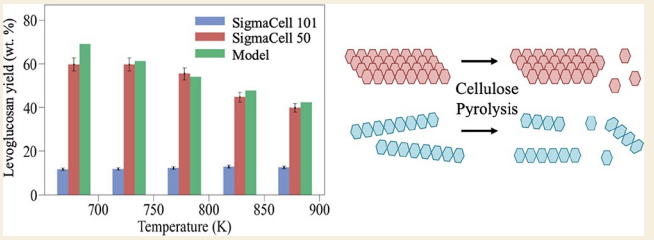

KEYWORDS: *cellulose, fast pyrolysis, micropyrolyzer, levoglucosan, kinetics, gas chromatography*

1. INTRODUCTION

Cellulose, which can constitute as much as 50% of lignocellulosic biomass, is a homopolymer made up of β-D-glucose molecules linked via β-(1 → 4) glycosidic bonds.[1] Intra- and interchain hydrogen bonding between the −OH functional groups of glucose and the ring or the glycosidic oxygen makes cellulose highly crystalline.[2,3] When subjected to fast pyrolysis, it primarily decomposes into levoglucosan (LVG) and a range of low-molecular weight products (LMWPs) such as glycolaldehyde (GA), glyoxal, furans, and gases by subsequent reactions.[4−6] Currently, LVG obtained from biomass is being assessed as a potential feedstock for synthesizing polyglucose, a prospective bioplastic.[7] GA is a prospective feedstock for producing biobased poly(ethylene terephthalate) (PET) and polyacetal thermoplastics.[8−10] Deconvoluting the underlying complex reaction pathways of cellulose pyrolysis could help tune desired product selectivities via feedstock selection, control of operating conditions, and catalytic routes to further aid in reactor design toward achieving those ends.

Py-GC-FID/MS experimental studies of cellulose, maltohexaose, cellobiose, glucose, and LVG pyrolyses have provided comprehensive information on the product distribution.[4−6] Anhydrosugars such as LVG-pyranose (ring closure between oxygen on C1 and OH group on C6), LVG-furanose (ring closure between oxygen on C1 and OH group on C4), anhydro-xylopyranose, 5-hydroxymethylfurfural (5-HMF), furfural, GA, formic acid, and CO_2 formulate a significant fraction of the pyrolysis vapors of cellulose.[5,6] With the decrease in DP, from cellulose to maltose (DP = 6), cellobiose (DP = 2), and glucose (DP = 1), the total yield of anhydrosugars drops significantly.[6] At the same time, relatively higher amounts of 5-HMF, char, and CO_2 were obtained.[6] Water yields in all the experimental studies have been estimated based on the yields of products usually formed via dehydration reactions due to the limitations of analytics.[5,6,11] Nevertheless, these studies enabled identifying the primary and secondary decomposition pathways of cellulose pyrolysis, which further allowed developing detailed reaction mechanisms. Briefly, cellulose

Received: February 1, 2022
Revised: March 22, 2022
Accepted: March 22, 2022
Published: April 5, 2022

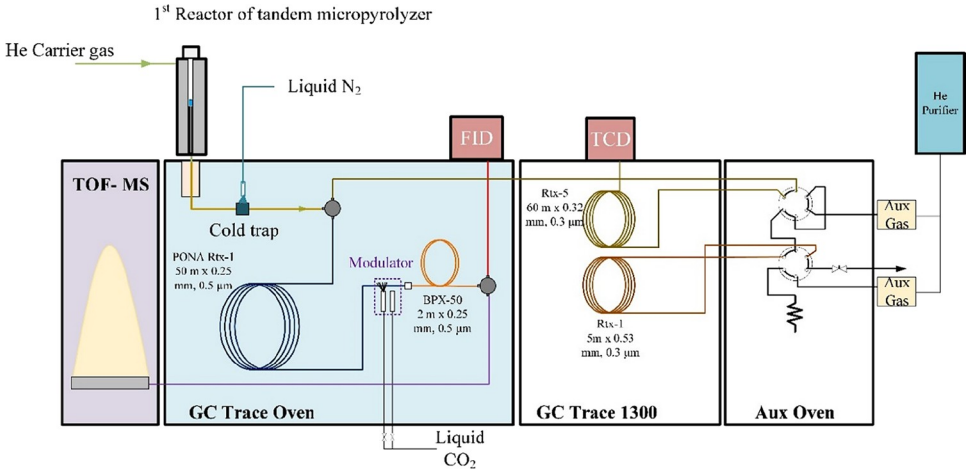

Figure 1. Schematic representation of the micropyrolyzer reactor with a comprehensive analytical section.

decomposition was assumed to be initiated either via end-chain scission or mid-chain dehydration, followed by glycosidic bond cleavages. The end-chain initiation of a nonreducing end releases an LVG unit, while a scission at the reducing end of cellulose forms a chain with the LVG end and a glucose molecule. The LVG end will further undergo depropagation, releasing more LVG. Dehydration and retro-Diels−Alder reactions of cellulose chains result in other anhydrosugars and LMWPs, which are not very prominent. Further, LMWPs such as 5-HMF, furfural, and GA evolve from glucose via a multistep series of reactions.[6,12]

The latest experimental investigations report that characteristic lengths of the sample, along with heating and cooling rates, could dramatically influence fast pyrolysis yields.[13] In general, the dimensionless numbers Py (Pyrolysis number) > 1 and Bi (Biot number) < 1 are desired to maintain a kinetic-controlled regime.[1] The transport map reported by Mettler et al. suggests that samples with characteristic lengths of <100 μm are favorable to maintain uniform isothermal conditions during pyrolysis experiments.[11] While the manufacturers of micropyrolyzers claim heating rate specifications on the order of 1000 K/s, the effective rates of sample cup heating are only about 400−500 K/s, as reported by Proano-Aviles et al.[14] In such cases, the method of introducing the sample may also influence product distribution. The pyrolysis yielded about 30−40 wt % of LVG when introduced as thin films with thicknesses of <70 μm as opposed to 50−60 wt % from the powders (50 μm) in a micropyrolyzer.[11,15] The most recently designed reactor for pulse-heated analysis of solid reaction kinetics (PHASR) claims to heat the sample in milliseconds at a rate of 11,000 K/s.[13] In PHASR, the samples are introduced as thin films, and the sample is expected to heat up instantaneously. LVG yields reported for PHASR experiments were as low as 10−15 wt %.[16] Such low yields of LVG have also been reported when there were substantial amounts of inorganics in commercial cellulose samples. Mineral salts (inorganics) have been found to catalyze cellulose conversion into furans by interacting with the oxygen present in the macromolecular chains and thereby lowering LVG formation significantly.[17−20] The binding of inorganic ions like Na^+ with cellulose chains could make mid-chain dehydration reactions around 90 times faster than neat cellulose.[18] However, the mechanistic reasoning for a substantial decrease in LVG yields from thin films remains unclear.

Another physical characteristic that reportedly affects the pyrolysis vapor composition is cellulose crystallinity. Pretreating cellulose could significantly reduce its crystallinity and, in some cases, cause a change in its allomorphic form.[21,22] It has been stated that the initiation of glycosidic bond cleavage occurs at amorphous sites of cellulose due to the absence of interchain hydrogen bonds.[23] Amorphous cellulose is reported to have a low onset thermal decomposition temperature (~513 K) with a char yield at least 5 wt % higher than the crystalline one.[24−27] It has been postulated that the crystallinity and crystal size influenced the activation energy of cellulose thermal decomposition.[25,28] However, this contradicts Broido et al.'s theory of amorphous cellulose chains recrystallizing before starting to depolymerize.[23] While a few studies found no noticeable effects of crystallinity on the yields of pyrolysis products, some report reduced LVG formation with a decrease in crystallinity and change in crystal allomorph.[15,27,29,30] A few researchers attribute this reduction in LVG to the reduced particle sizes due to pretreatment techniques such as ball-milling.[15] It is therefore imperative to have a more comprehensive understanding of the role of cellulose crystallinity on pyrolysis product yields.

To this end, this work aims to deconvolute the effects of particle size (~20 and 50 μm) and crystallinity on cellulose pyrolysis through a combination of experiments using two different commercial celluloses and kinetic modeling. The pyrolysis experiments are performed on a micropyrolyzer coupled with comprehensive 2D-gas chromatography (GC × GC) and a customized GC to analyze LMWPs, gases, and water fractions simultaneously. Accurate analysis of water yield will also assist in validating the extent of dehydration reactions in the kinetic model. Shallow eco-cups and high sweep gas flow rates are used to reduce the diffusion effects and secondary reactions of the volatilized products. The detailed product profiles obtained for all the types of cellulose and model compounds are interpreted by modifying the detailed kinetic model developed by Zhou et al.[6,12] to rationalize the new findings of this work. A plausible mechanism for the reduction of observed LVG yields from amorphous celluloses is also proposed.

https://doi.org/10.1021/acsengineeringau.2c00006
ACS Eng. Au 2022, 2, 320−332

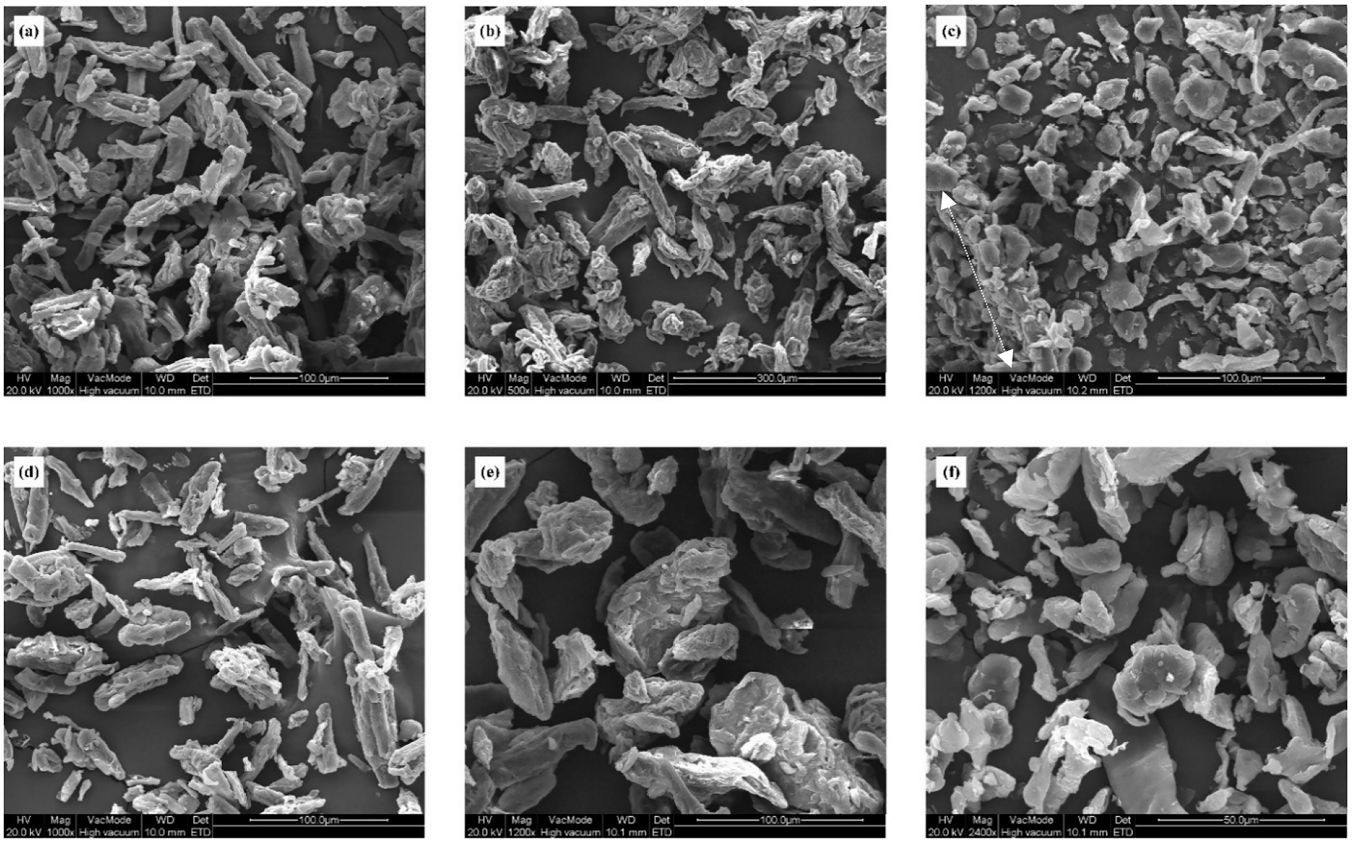

Figure 2. Scanning electron microscopy (SEM) images of (a) SigmaCell Type 20 (mag. 1000×, 100 μm spatial resolution), (b) SigmaCell Type 50 (mag. 500×, 300 μm spatial resolution), and (c) SigmaCell Type 101 (mag. 1200×, 100 μm spatial resolution). (c) Arrow indicates a cluster or aggregate of particles formed due to high amorphous content in the sample. Differences in the surface morphology and particle shapes can be seen in (d) SigmaCell Type 20 (mag. 1000×, 100 μm spatial resolution), (e) SigmaCell Type 50 (mag. 1200×, 100 μm spatial resolution), and (f) SigmaCell Type 101 (mag. 2400×, 50 μm spatial resolution), respectively.

2. MATERIALS AND METHODS

2.1. Materials

Cellulose substrates, viz., SigmaCell Types 20, 50, and 101, cellobiose, β-D-glucose, and 1,6-anhydro-β-D-glucose (LVG) were purchased from Sigma-Aldrich. According to the purchase label, SigmaCell Types 20 and 50 have average particle sizes of 20 and 50 μm, respectively. On the other hand, SigmaCell Type 101 is composed of highly purified cellulose fibers and has an average particle size of 15−18 μm. Calcium carboxylate monohydrate for the calibration of CO and CO_2 gases was also purchased from Sigma-Aldrich. Deionized water with a conductivity of <0.01 S/m was used for calibrating its fraction in the pyrolysis vapors.

2.2. Sample Characterization

The peak deconvolution method was applied to determine the crystallinity of cellulose samples. Crystallinity indices of cellulose samples were obtained with the help of X-ray diffraction (XRD) on a Siemens Diffractometer Kristalloflex D5000 using Cu K_α radiation. The powder patterns were collected in a 2θ range from 10 to 90° with a step of 0.04° and 30 s acquisition per angle. Scanning electron microscopy (SEM) was applied using an FEI Quanta 200 F apparatus to probe the particle size distribution, operating at 20 kV. The sample was spread on carbon tape and sputter-coated with a layer of gold (<5 nm) to suppress charging. Images obtained at various magnification levels were then processed using ImageJ software to get the particle size distribution.

2.3. Micropyrolyzer Unit

As described previously, the experiments were performed with a double-shot tandem micropyrolyzer.[31] Only the first reactor was used in this work. It is directly connected to the GC inlet to perform solid-to-gas experiments in this study. Briefly, the cryotrap was cooled up to 77 K using liquid N_2 for 5 min to collect all the vapors. The product vapors were split using a Y-type column connector to analyze gases and water simultaneously in a customized GC and LMWPs in the GC × GC. The gases, i.e., CO, CO_2, and water, were separated on an Rtx-5 capillary column connected to a thermal conductivity detector (TCD). The GC × GC consists of Rtx-1 PONA and BPX-5 columns connected in series, with liquid CO_2 modulation jets. An ionization voltage of −20 eV was applied to enable accurate identification in the TOF-MS for product identification. A flame ionization detector (FID) was connected to the GC × GC for quantifying the product yields. A schematic of the setup modified for cellulose fast pyrolysis experiments is shown in Figure 1.

Shallow eco-cups loaded with 100 − 150 μg of the samples were introduced into the pyrolyzer and flushed with helium for 0.5 − 1 min, after which they were dropped into the preheated reactor (673−873 K). SigmaCell Type 20, cellobiose, and glucose were pyrolyzed only at 773 K. Each experiment was performed in replicates of two, and the results were within 5% margin of error. As the obtained char weighed below the detectable limits of the microbalance, 350−400 μg of cellulose samples were pyrolyzed separately to determine the char yields. A split flow of 210 mL/min with a split ratio of 100:1 was maintained to sweep the product vapors from the reactor and avoid secondary reactions. A modulation time of 7 s was chosen to obtain a better resolution in the GC × GC. The temperature profiles measured in the reactor and GC programs are provided in the SI.

LVG samples of varying masses were vaporized to obtain a calibration chart (R^2 > 0.98). Similarly, deionized water was injected into the GC at different volumes to calibrate the customized GC (R^2 > 0.98). Known amounts of calcium oxalate were pyrolyzed at 1073 K to calibrate the GC for CO and CO_2 according to stoichiometry (R^2 >

https://doi.org/10.1021/acsengineeringau.2c00006
ACS Eng. Au 2022, 2, 320−332

0.99). All other LMWPs were quantified according to the effective carbon number method (as described by Pyl et al.[32]). The relative response factor of LVG relative to fluoranthene was determined using the effective carbon number method. Further, LVG yields are calculated from the calibration chart, which is then used as an internal standard to quantify other compounds with the help of eq E1.

$$W_i = \frac{f_i V_i}{f_{st} V_{st}} W_{st} \quad \text{(E1)}$$

Here, W_i and W_{st} represent the mass percentages of a species i and the internal standard, respectively. f_i and f_{st} correspond to the relative response factors of species i and the internal standard, while V_i and V_{st} represent the blob volumes of these compounds obtained from the 2D chromatograms.

2.4. Reaction Mechanism

The detailed cellulose thermal decomposition model published from Zhou et al. has been adopted to mechanistically assess the experimental yields obtained in this work.[6,12,33] Briefly, this model was originally developed based on continuous distribution kinetics and comprised 342 reactions and 102 species. Thermal decomposition reactions include end-chain initiation, dehydration, thermohydrolysis, 1,2-dehydration, retro-Diels–Alder reaction, mid-chain dehydration, and secondary fragmentations. The model assumes glucose to be the intermediate species during cellulose pyrolysis, which further reacts via dehydration, ring-opening/closing, isomerization, retro-Diels–Alder reaction, retro-aldol reaction, keto-enol tautomerism, and cyclic/Grob fragmentation. The high sweep gas rates employed in a micropyrolyzer to minimize higher-ranked reactions by continuously removing the volatile products out of the reactor are accounted for. The pre-exponential factor (A) and activation energy (E_a) for each reaction were derived from experimental or theoretical calculations. The rate equations are automatically generated (with the help of programs developed in Perl and C++) using mass action kinetics, which are solved as a function of time using DDASAC.[34] The initial mass fraction, average molecular weights of cellulose, temperature, and rate parameters were provided as inputs.

3. RESULTS AND DISCUSSION

3.1. Cellulose Characterization

SEM was used to examine the variations in surface morphology and particle size distributions of different types of SigmaCell cellulose. Figure 2a–c shows that Type 20 and 50 cellulose materials have distinct, rod-shaped fibrous particles. In contrast, Type 101 appeared to be irregularly shaped thin wafers or particles. The particles of the Type 101 material also appeared to be in the form of aggregates marked by an arrow in Figure 2c. This observation is noticeably similar to the darkfield microscopic evaluations wherein phosphoric acid-swollen cellulose with low crystallinity tended to form aggregates of particles.[27] Due to the hygroscopic nature of amorphous cellulose, its particles tend to absorb moisture, which then forms a binding film between the adjacent particles. Such a phenomenon drives the particles to form aggregates under ambient conditions. It could be qualitatively established that Type 101 is highly amorphous at this stage. From a higher-magnification image (Figure 2f, 2400×), it is apparent that these particles exhibit a much smoother surface with no visible pores. Size reduction techniques such as milling generate ultrafine powders with very smooth surfaces.[35] On the contrary, Types 20 and 50 have irregular surfaces with relatively large pores in the particles, especially in Type 50, as shown in Figure 2d,e. In addition to the differences in surface morphology, significant differences in the characteristic lengths were observed.

At least 100 particles were processed from the images in Figure 2a–c with magnifications of 1000×, 500×, and 1200× to determine the average particle sizes by measuring the longest dimension of each particle listed in Table 1. Gamma distribution was obtained based on the histograms, with the data presented in Figure 3. Although the Type 20 purchase label specifications claim to have particles of 20 μm, the average size was closer to 40 μm. Type 50 material has a broad distribution of particles with an average characteristic length of 50 μm and a few as large as 180 μm. In contrast, a narrow distribution was observed for Type 101 with the average size ranging between 10 and 20 μm.

Table 1. Physical Properties of the Three Types of Cellulose Substrates Used in this Work

cellulose substrate	average particle size (μm)	crystallinity index (%)	degree of polymerization[a] (no. of units)
SigmaCell Type 20	34.90	91.60	168
SigmaCell Type 50	57.51	90.06	165
SigmaCell Type 101	16.96	45.43	442

[a]Obtained from Deneyer et al.;[36] based on viscosimetry measurements.

X-ray diffractograms from all three substrates indicating the characteristic crystallographic planes of cellulose I are presented in Figure 4. Changes in crystallinity are evident from the disappearance of planes ($\bar{1}10$), (110), and (004), along with the reduction in peak height of plane (200) in SigmaCell Type 101. Crystallinity indices calculated based on the peak deconvolution method and listed in Table 1 suggest that Types 20 and 50 have a very high density of crystalline regions. The XRD study shows that Type 101 is nearly 50% amorphous, supporting the qualitative observations of the SEM. Such a high amorphous content would reduce the maximum decomposition temperature considerably and may influence the reactions of cellulose pyrolysis.

3.2. Effect of Particle Size and Crystallinity on Pyrolysate Composition

The GC × GC-FID chromatograms obtained for SigmaCell Types 50 and 101 pyrolysis experiments at 773 K are shown in Figure 5a,b. The results of SigmaCell Type 20 were comparable to Type 50 in terms of pyrolysate composition, and therefore, SigmaCell Type 50 has been chosen as a representative for crystalline cellulose. About 60 species were identified on GC × GC-FID and customized GC-TCD for all types of celluloses, which were separated depending on their boiling points and polarities. All detected product species and their associated product yields are listed in Tables S2 and S3 of the SI. The GC × GC technique was instrumental in separating many compounds, such as anhydrosugars (with a MW of 144) and 5-HMF with similar boiling points. GA peaks are observed at several retention times, which are confirmed by mass spectrometry, possibly due to its interaction with the stationary phase or oligomerization into dimers or trimers. While there are predominant anhydrosugar peaks seen in the chromatogram of SigmaCell Type 50, many smaller peaks of LMWPs were detected for Type 101.

LVG-pyranose was identified as the dominant species in the pyrolysis vapors of Type 50, which decreased from 60 to 40 wt

https://doi.org/10.1021/acsengineeringau.2c00006
ACS Eng. Au 2022, 2, 320–332

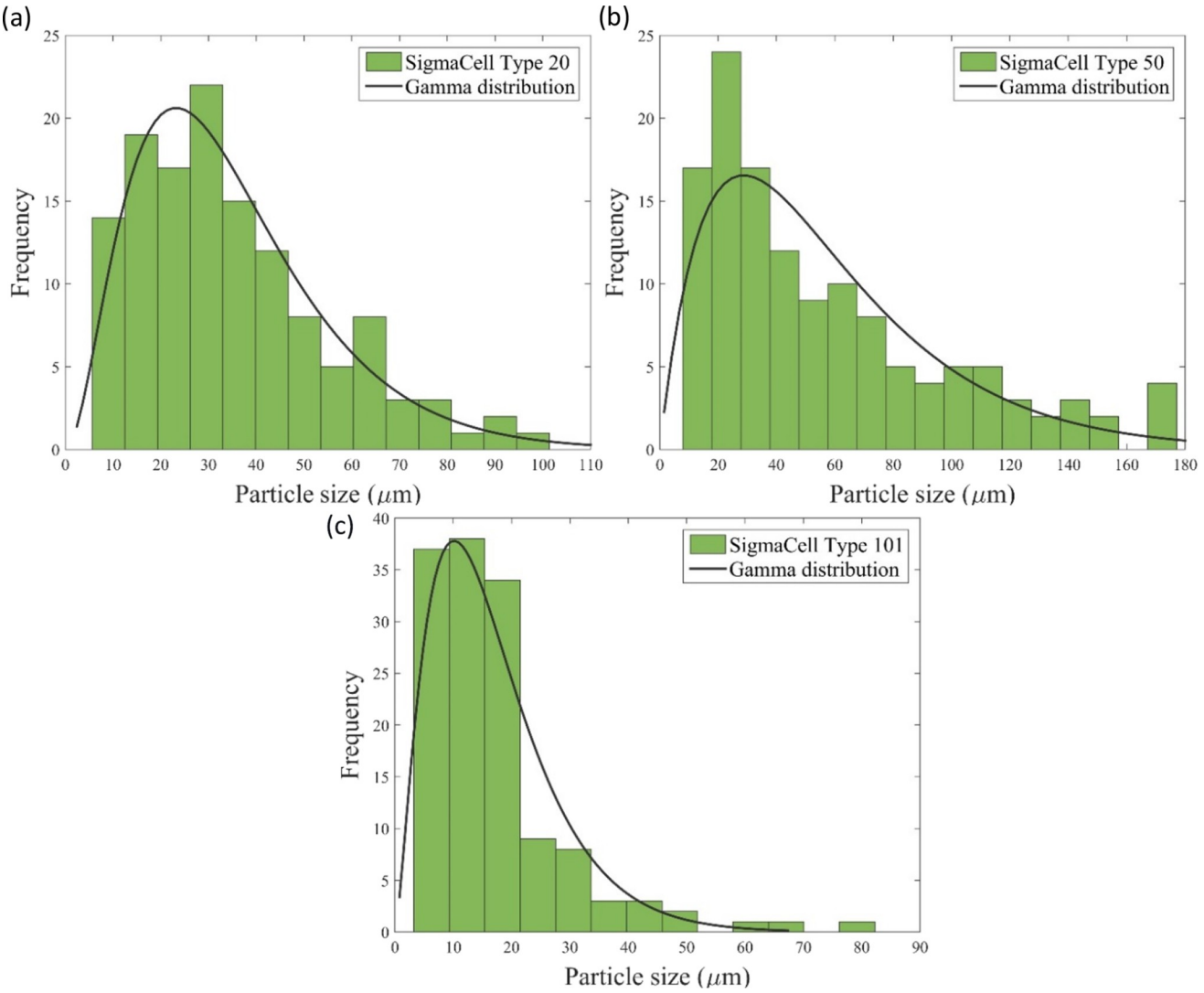

Figure 3. Histograms and particle size distributions of the three types of SigmaCell. (a) Type 20 particles range from 0 − 120 μm; (b) Type 50 particles range from 0 − 180 μm; (c) Type 101 particles range from 0 − 80 μm. At least 100 particles from SEM images of each type were processed using ImageJ software. The frequency curve (black line) represents the gamma distribution of the particles.

% as the temperature increased from 673 to 873 K, as shown in Figure 6a. These results are consistent with the experiments and the kinetic model reported by Zhou et al.[12] According to the mechanism proposed by Zhou et al.,[12] LVG is formed mainly from the end-chain initiation reactions, glucose dehydration, and chain depropagation reactions (Figure S2 in the SI). Reduced yields of LVG at high temperatures are due to the activation of competing reactions that generate LMWPs—these typically have higher activation energies made accessible at elevated temperatures.[12] The same trend was observed for LVG-furanose, which is formed by the dehydration of a furanose isomer of glucose (Figure S4 in the SI). This implies that the competing pathways leading to some major LMWPs like GA, 5-HMF, furfural, and methylglyoxal require an intermediate formed via a high kinetic barrier, while subsequent decomposition reactions are quite fast. Accordingly, higher yields of these species were observed at temperatures 823−873 K, which are in close agreement with the kinetic model (data taken from Zhou et al.[12]), as shown in Figure 6. The other significant products were anhydrosugars like anhydro-xylopyranose and a few species with MWs of 162 and 144, whose identity could not be established entirely based on the MS databases (listed in Table S2 of the SI). Contrary to the model results, the experimental GA yields were relatively low (<5 wt %) at 673−773 K and increased nearly threefold beyond 773 K. The disagreement between the model and experiments could potentially be attributed to two factors: (i) better resolution by GC × GC relative to 1D GC and (ii) underestimated kinetic parameters corresponding to retro-aldol or retro-Diels−Alder reactions in the kinetic model.

Although disagreements exist in GA yield between model results and experiments, generally good agreement was observed for a range of LMWP pyrolysate components. An important highlight of this work is the reasonably good match between the water yields and the model predictions (Figure 6b). In the experimental work of Zhou et al.,[6] water yields were estimated based on the combined yield of dehydration products, which fell short of the model-predicted values. With accurate detection of water present in the pyrolysis vapors, the experimental data seemed to have a better agreement with the model (Figure 6c). Further, trends of some of the minor LMWPs (yields of <1 wt %), like furanmethanol, are shown to be in line with the model-predicted values (Figure 6h). The sum of the yields of the

https://doi.org/10.1021/acsengineeringau.2c00006
ACS Eng. Au 2022, 2, 320−332

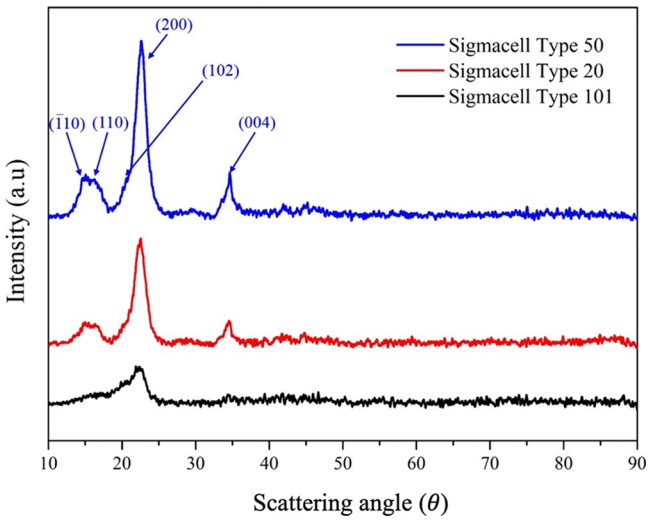

Figure 4. XRD diffractograms of the three different celluloses: SigmaCell Types 20, 50, and 101. The disappearance of characteristic peaks of the crystallographic planes corresponding to scattering angles 14.7, 16.1, and 35° along with a shortened peak at 22.5° indicate reduced crystalline fractions in SigmaCell Type 101.

measured products using gas chromatography for the experiments at temperatures 673−773 K was close to 93−95 wt %, and at 823 and 873 K, this reduced to 89 and 86%, respectively. The reduction in the measurable species could be attributed to the volatilization of oligomers, which cannot be detected by the GC × GC.

Pyrolysis of Type 101 cellulose produced markedly low yields of LVG, ranging between 10−15 wt % at temperatures of 673−873 K (Figure 6a). The values are comparable with those reported for thin-film pyrolysis in PHASR (Figure 7).[16] LVG formation seemed to be nearly independent of temperature as the yields remained stable. To verify its secondary decomposition, pure samples of LVG were vaporized, and a single peak was detected at a retention time corresponding to LVG. This could mean that the reactions producing LVG have competing pathways in the case of Type 101, which could be attributed to its smaller particle size distribution or lower crystallinity.

On the other hand, GA and water yields increased significantly compared to Type 50 (Figure 6b,c). A nearly 8% (by weight) increase in the GA yields at 673 K implies that the energy barriers of the corresponding reactions are substantially more accessible relative to other allomorphs. Retro-aldol and retro-Diels−Alder reactions that generate GA might be the competing pathways of LVG formation even at low temperatures. Moreover, water yields increased twofold compared to the measured values of Type 50 (Figure 6c), which originates from the enhanced dehydration reactions. It is also plausible that the initial samples had adsorbed significant quantities of water and resulted in water-mediated chemistry. The presence of water has been postulated to affect multiple reaction families, affecting reaction barriers for chemistries involving hydrogen transfer reactions such as ether bond cleavage, dehydration, retro-aldol fragmentation, and others.[33]

Unlike SigmaCell Type 50, small amounts of anhydrosugars were observed, similar to the reduced LVG yields (Table S3 of the SI). This suggests that the dehydration reactions do not result in significant anhydrosugar production from either cellulose chains or glucose units. Mid-chain scissions involve dehydration at random sites on the cellulose chains and further fragmentation to produce two smaller chains with LVG ends, which are not detected by the GC × GC. If the estimation methods were used to calculate water yields, it would have underestimated the extent of dehydration reactions via this indirect method. The composition of other species like 5-HMF (Figure 6d), acetone, and formaldehyde in the effluent remained similar to the observed products in pyrolysis of Type 50 cellulose (listed in Tables S2 and S3 of the SI). The observations imply that the glucose decomposition pathways leading to the formation of these species remain unaltered. The yields of CO_2 were found to be slightly higher than those from Type 50 pyrolysis, while its experimental dependency on temperature is comparable (Figure 6e). The trends of methylglyoxal yields with increasing temperature were also similar to type 50 (Figure 6h). However, its yields were observed to increase 2−3 times in the case of Type 101. Furanmethanol, formed from 5-HMF via decarbonylation, was observed to increase by an order of magnitude compared to Type 50 (Figure 6g). In line with this, CO yields increased drastically with temperature, suggesting more pronounced decarbonylation reactions in the case of Type 101 (Figure 6f).

As mentioned earlier, more furanic species were identified in the pyrolysis vapors of SigmaCell Type 101. Compared with the earlier case, there was a less than 1% difference among their total mass yields, suggesting minor alternative pathways that generate furanic species. However, the sum of the GC-quantifiable yields using the internal standard method at low temperatures (673 and 723 K) was between 60 and 65 wt %, which increased up to 80 wt % at 873 K. This indicates that there may have existed heavier oligomeric compounds with higher boiling points that cannot be detected by gas chromatography. Above all, the reaction mechanism of the thermal decomposition to Type 101 cellulose seemed to be perturbed to a large extent. Table 2 shows the yields of all the major product species of SigmaCell Types 50 and 101, cellobiose, and glucose at 773 K. It was observed that the amounts of LVG, GA, water, and CO_2 formed from the Type 101 cellulose and glucose were quite comparable. This could indicate that the initial thermal decomposition of cellulose of Type 101 proceeds significantly via glucose formation instead of LVG.

To ascertain the reasons for the notable differences in the two types of celluloses, SigmaCell Type 20 with an average particle size of 35 μm was pyrolyzed at 773 K. If the LVG yields were significantly influenced by the particle size, the expected yield values would be expected to be in the range of 10−50 wt %, based on this hypothesis, as the particle size distribution for Type 20 lies between Types 50 and 101. As shown in Figure 7, the measured values of LVG yield are similar to that of Type 50 (∼50 wt %), which is consistent with the experimental work of Zhang et al.[15] Moreover, the crystallinity indices measured for the samples of Types 20 and 50 are about the same (∼90%). Based on these arguments, it can be established that crystallinity is the influencing factor for the low LVG formation by promoting alternative pathways of cellulose thermal decomposition. These observations also support the work of Kim et al.,[29] who inferred that the presence of hydrogen bonding and van der Waals forces might influence the initial thermal decomposition of cellulose. The extent of hydrogen bonding varies in different allomorphs wherein the sheets of cellulose chains are stacked in a parallel or antiparallel fashion in a three-dimensional crystal structure.

https://doi.org/10.1021/acsengineeringau.2c00006
ACS Eng. Au 2022, 2, 320−332

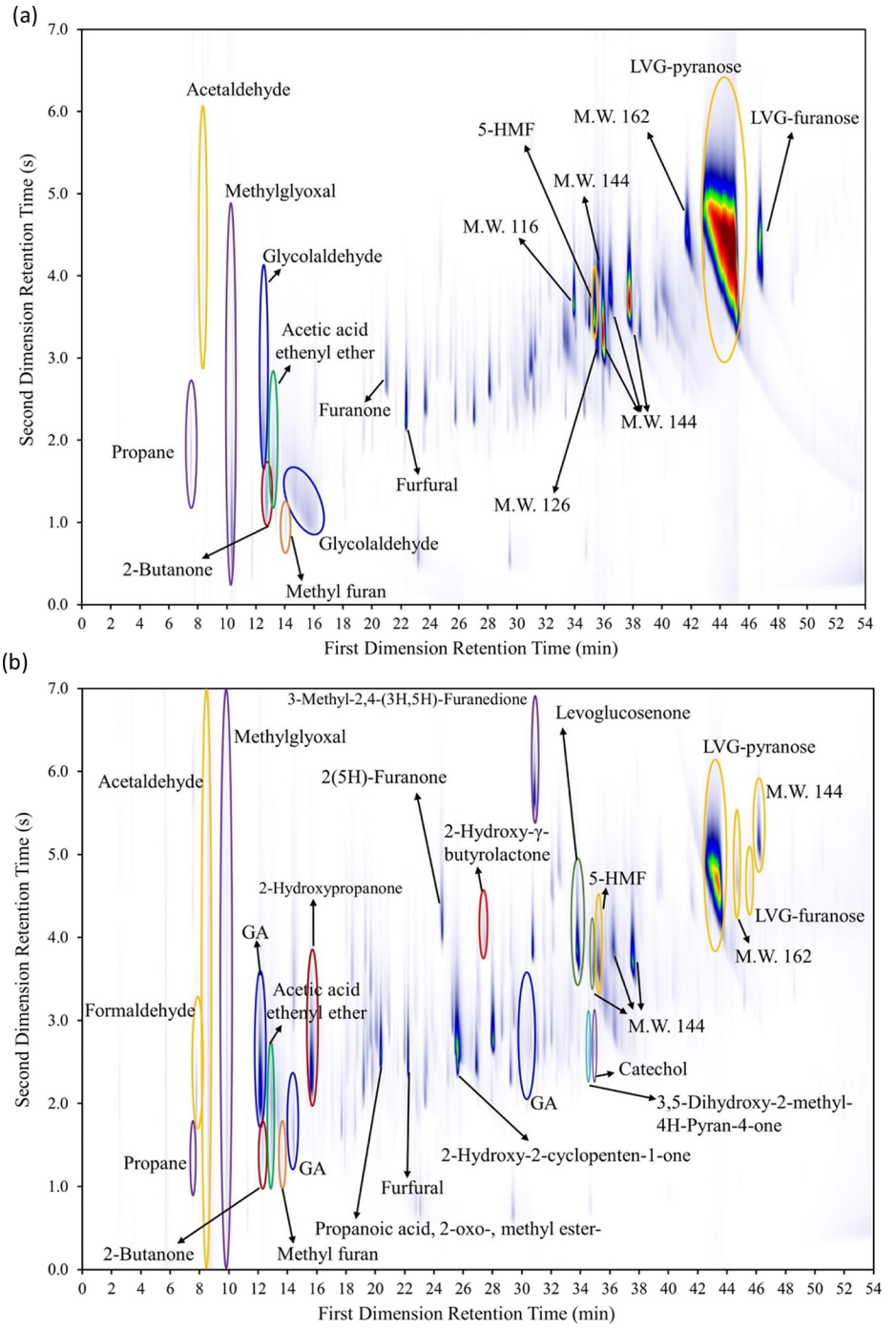

Figure 5. Py-GC × GC-FID pyrograms obtained for (a) SigmaCell Type 50 and (b) SigmaCell Type 101 at 773 K.

Further, Mukarakate et al.[27] reported that cellulose samples with low crystallinities produced smaller amounts of LVG, which also depended on the kind of allomorph that was pyrolyzed.

3.3. Physical Characteristics of Pyrolysis Char

The char mass yields obtained from cellulose Types 50 and 101 were very low, around 5−7 wt %. The physical characteristics of char that was left behind in the sample cup appeared extremely different. Type 50 cellulose deposited a thin black layer on the bottom surface of the cup upon pyrolysis at 773 K. The char layer appeared to be very sticky on the surface of the sample cup, with signs of bubble formation (that must have occurred during pyrolysis). It is evident from Figure 8a that these particles underwent an intermediate molten (or liquid) stage.

Char obtained from the pyrolysis of Type 101 particles was a black solid, as shown in Figure 8b. It appeared to be very brittle and easily separated from the cup (Figure 8c) without leaving any residue on the sample cup, which is entirely different from the highly crystalline samples. It is interesting to note that these observations are also similar to the thin-film pyrolysis at 773 K as reported by Krumm et al.[37] It is plausible that the amorphous chains undergo rapid mid-chain fragmentation and dehydration reactions, resulting in the

https://doi.org/10.1021/acsengineeringau.2c00006
ACS Eng. Au 2022, 2, 320−332

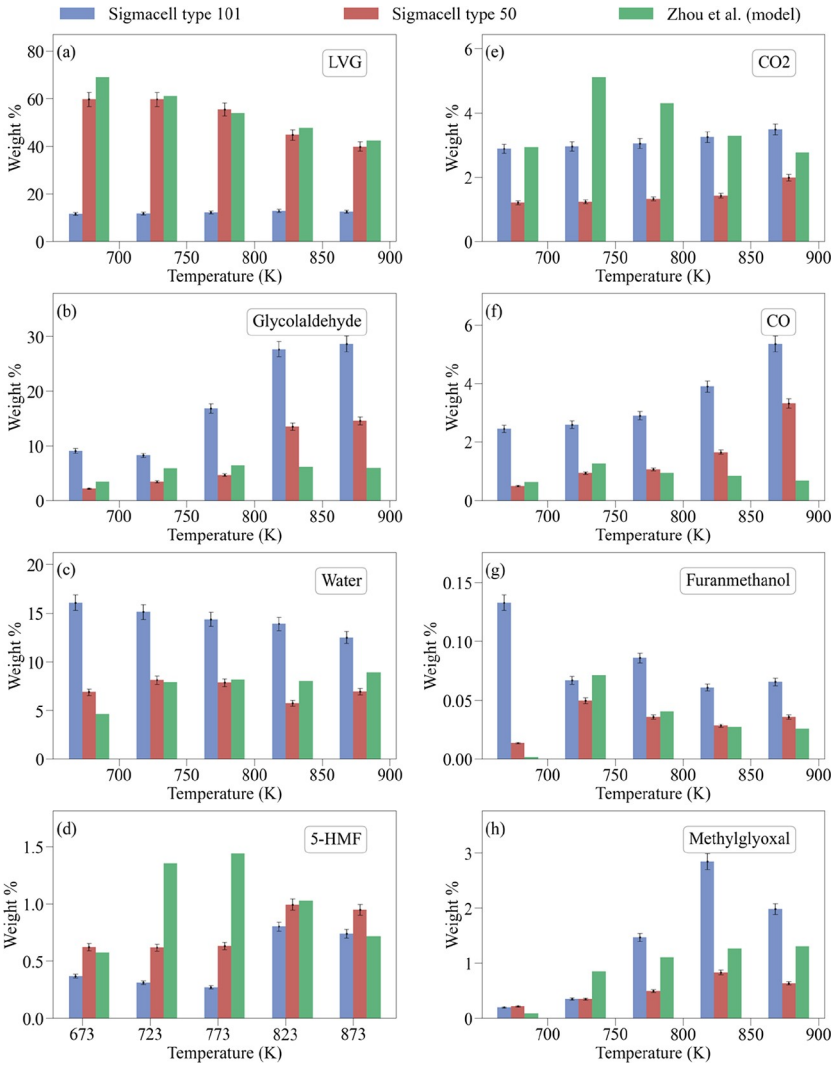

Figure 6. Experimental yields of some of the LMWPs obtained from SigmaCell Types 101 and 50 as well as the model predictions of Zhou et al.[12] The experimental error percentage is of the order of 5%.

formation of oligomers that either remain in the solid phase or volatilize in the form of aerosols.[38−40]

3.4. Mechanistic Understanding of Low LVG Formation

To better understand the effect of cellulose allomorph type on the pyrolysate composition, we examined specific elementary steps in the reaction network of cellulose decomposition. From a thermodynamic point of view, the dissociation energies of the H bonds (20 kJ/mol) and energetics of the van der Waals interactions (12 kJ/mol) are at least an order of magnitude lower than the dissociation energies of glycosidic bonds, implying that the crystalline structures decompose in a facile fashion under fast pyrolysis conditions.[26] Hosoya and Sakaki demonstrated that the mid-chain decomposition of a single hexamer chain is the most favorable as it involves no intrachain hydrogen bond breaking.[41] The mid-chain cleavage of the hexamer results in two shorter chains, one with a reducing end and the other with an LVG end ($E_a \approx 159$ kJ/mol). However, the depropagation reactions are the least favorable pathways, in terms of higher E_a values, around ∼197 kJ/mol. In this case, LVG is not instantaneously volatilized, and it might undergo secondary decomposition in the solid phase. Hosoya and Sakaki further report that these reactions are more prominent in amorphous celluloses at temperatures of 200−280 °C.[41] In a three-chain model, not only the hydrogen bond energies but also the binding energies between the chains become significant. Due to this, the activation energies for the mid-chain scissions at the center of the crystal have substantially higher barriers ($E_a \approx 334$ kJ/mol) than the scission on the surface ($E_a \approx 250$ kJ/mol).

Further, the barrier height for the depropagation reaction is only 215 kJ/mol, which results in an increase of LVG units formed. This implies that if cellulose has a mix of crystalline and amorphous phases, pyrolysis of the former would be expected to result in increased LVG yields. In contrast, the latter would not result in high LVG yields due to the absence of interchain interactions that would otherwise favor the formation of LVG. Inspired by the study of Hosoya and Sakaki, the activation energies for mid-chain dehydration reactions were lowered by 18.8 kJ/mol, and mid-chain fragmentations by 5.9 kJ/mol as each hydrogen bonding in cellulose crystalline structure was reported to stabilize the energy by 8−20 kJ/mol. The modified parameters and the original values are reported in Table 3. The pathways are highlighted by bold arrows in Figure 9.

The adjusted kinetic parameters for mid-chain reactions significantly affected the model-predicted yields of the

https://doi.org/10.1021/acsengineeringau.2c00006
ACS Eng. Au 2022, 2, 320−332

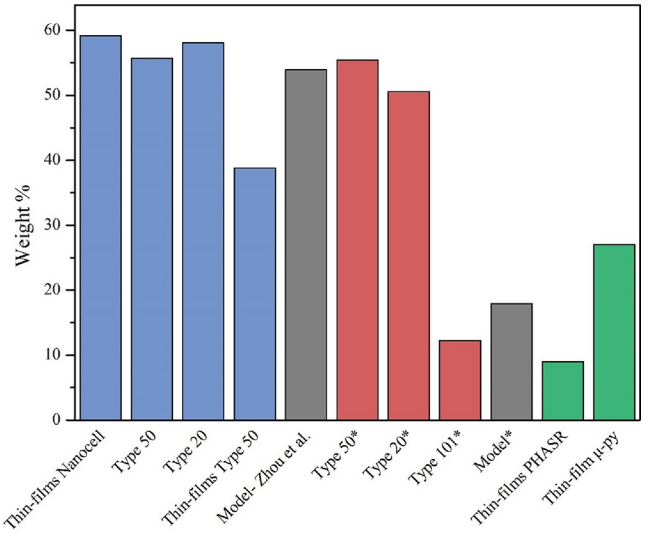

Figure 7. Comparison of LVG yields obtained in this work with literature for cellulose pyrolysis at 773 K. Data for Thin films Nanocell, Type 50, Type 20, and Thin films Type 50 are taken from Zhang et al.[15] Model yields were reported by Zhou et al.[12] Data for Thin-films PHASR and Thin-films μ-py are taken from Maduskar et al.[16] Type 50*, Type 20*, and Type 101* are the yields obtained in this work. Model* is the one with modified Arrhenius rate parameters discussed in Section 3.4.

Table 2. Comparison of the Mass Yields (wt %) of Major Low-Molecular Weight Species Obtained from Different Feeds, viz., Glucose, Cellobiose, and the Two Types of Celluloses, Type 50 and 101, Obtained at 773 K

product species	glucose	cellobiose	SigmaCell Type 101	SigmaCell Type 50
CO	1.27	0.50	2.90	1.06
CO_2	3.04	1.21	3.05	1.33
water	14.21	6.89	14.37	7.87
LVG	9.83	40.08	11.57	57.64
furfural	1.20	0.76	0.40	0.25
5-HMF	2.97	1.02	0.20	0.62
GA	12.69	1.23	15.06	3.44

significant product fractions. The LVG yield was reduced substantially (11−20 wt %) by increasing the mid-chain reaction rates, which corresponded with the increased water yields, as shown in Figure 10a,c. This indicates that the absence of intrachain hydrogen bonding (amorphous cellulose), which is reflected by lowered activation energies of mid-chain reactions, could be a potential reason for the reduced yields of LVG. The presence of hydrogen bonds in crystalline cellulose favors end-chain reactions, resulting in higher amounts of LVG. While the model-predicted LVG yields are still higher than the experimental values of SigmaCell Type 101, there is a qualitative agreement between the experiments and the modified model for the formation of water (Figure 10c). At the end of the pyrolysis simulations, the total polymer, LMWP, and melt phase yields were about 20, 60, and 19 wt %, respectively, at temperatures in the range of 673−823 K. On the contrary, polymers were less than 1 wt %, and LMWPs contributed up to 92 wt % in the original model.

Table 3. Arrhenius Rate Parameters of Different Cellulose Decomposition Reactions[a]

	original model		modified model	
reaction type	E_a	A	E_a	A
mid-chain fragmentation (ii)	224	5.5×10^{14}	218	5.5×10^{14}
mid-chain 3,6-dehydration (i)	251	50×10^{15}	232	50×10^{15}
thermohydrolysis	142	1.0×10^{14}	251	1.0×10^{14}
mid-chain fragmentation (v)	224	5.5×10^{14}	218	5.5×10^{14}
mid-chain 3,6-dehydration (iv)	251	5.0×10^{15}	232	5.0×10^{15}

[a]Values for E_a are reported in kJ/mol, and values for A are reported in s^{-1} or M^{-1} s^{-1}.

According to the reaction mechanism proposed by Zhou et al.,[6,12] increased mid-chain dehydration reactions also increase the formation of glucose, a key intermediate in the formation of the LMWPs. The model captures the formation of methylglyoxal from the D-glucose intermediate reasonably well, as shown in Figure 11d. However, there is an apparent disagreement between the model and experiments for GA, as shown in Figure 11b. A few computational studies reported the influence of interchain hydrogen bonding interactions on the activation energy barrier of glycosidic bond cleavage.[42,43] To obtain more insights into this, the activation energies of the retro-aldol reactions of pyrolysis reactions originating from glucose (that are known to form GA) were lowered by 7.1 kJ/mol. This change in activation energy resulted in a twofold increase in GA yields (Figure 11a).

At lower temperatures, 673 and 723 K, the total yields of GA match with the experimental data, but that is not the case at

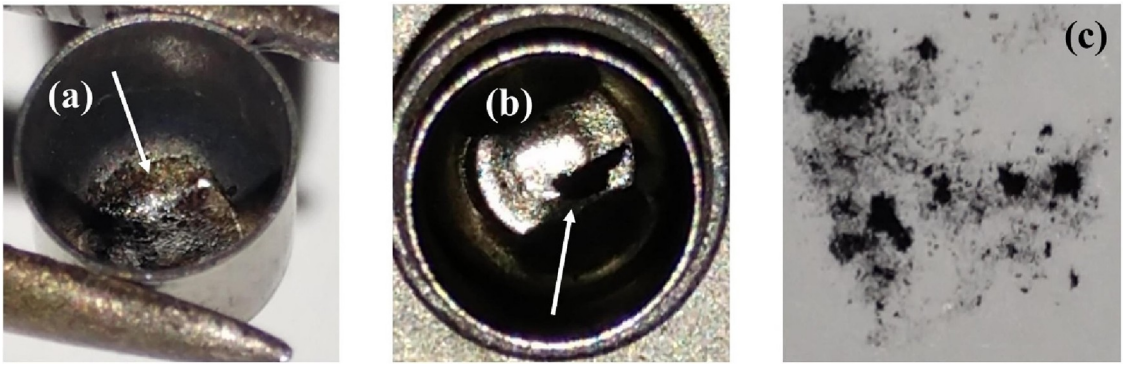

Figure 8. Different types of char formed at 773 K: (a) sticky layer of char on the bottom of the sample cup formed during cellulose Type 50 pyrolysis; (b) solid char particles formed during cellulose Type 101 pyrolysis, leaving a clean surface on the cup; (c) brittle char obtained from cellulose Type 101.

https://doi.org/10.1021/acsengineeringau.2c00006
ACS Eng. Au 2022, 2, 320−332

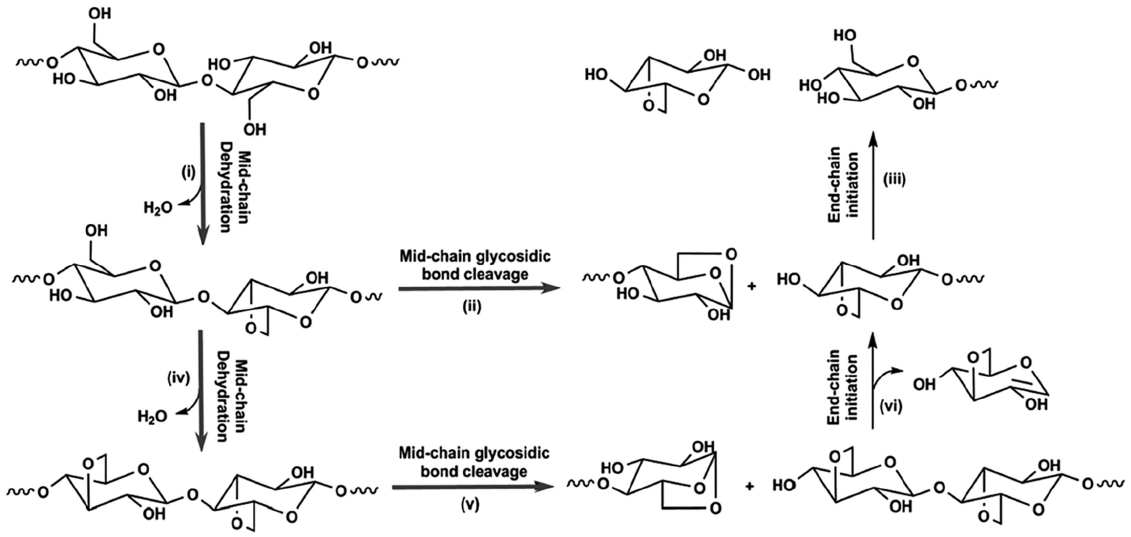

Figure 9. Decomposition mechanisms of the mid-groups in cellulose chains. Adapted with permission from ref 12. Copyright 2014 American Chemical Society.

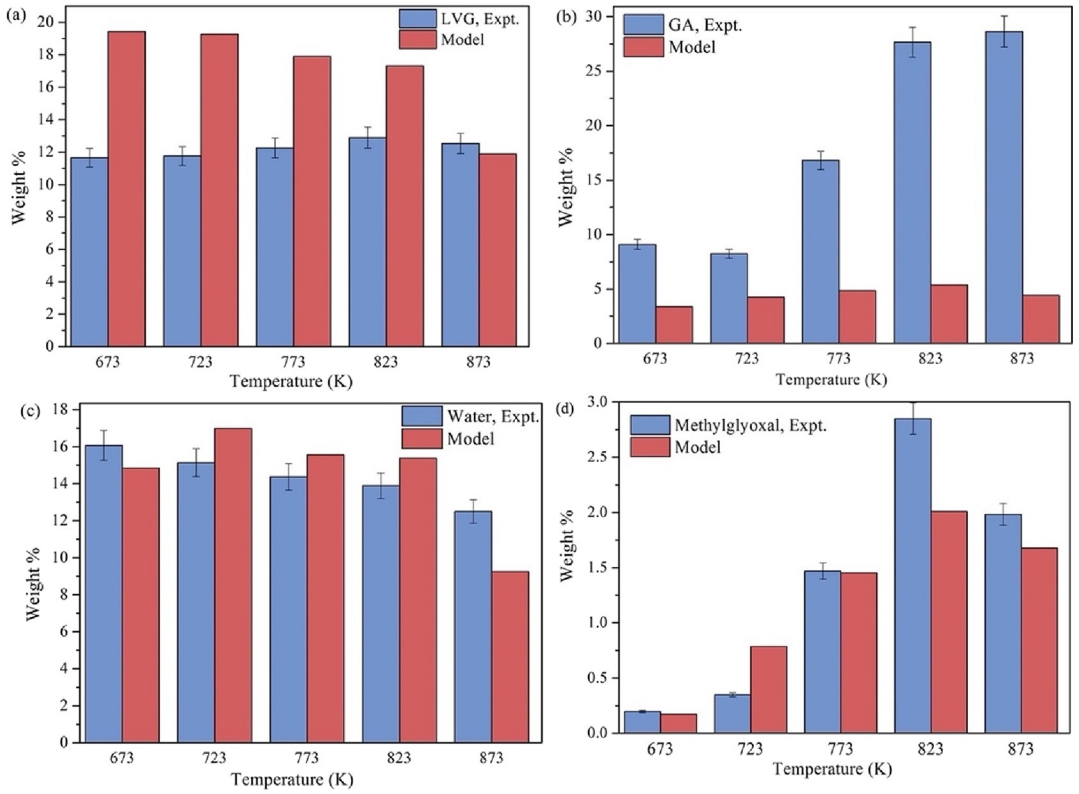

Figure 10. Comparison of LMWP yields of the modified model with experimental yields of Type 101 pyrolysis.

higher temperatures (Figure 11a). The rate of production analysis reveals that the retro-aldol reactions of species formed via the D-glucose intermediate (reactions 44, 48, 49, and 69 in Schemes S4 and S5) are primarily resulting in the formation of GA, followed by retro-Diels–Alder reactions from cellulose chains (reactions VII and XII in Scheme S2), dehydrated glucose-enol, glucose-enol, and precyclic hydroxy lactone (reactions 5, 9, and 61 in Schemes S4 and S5) as shown in Figure 11a. Net rate analyses of each of the reactions that produce GA are presented in Figure 11b for a pyrolysis temperature of 773 K. It was found that the retro-aldol reaction of D-glucose (reaction 44 of Scheme S4) is the fastest. The second fastest reaction is the retro-aldol reaction of erythrose (reaction 48 of Scheme S5). Due to the higher yields of D-glucose from the modified model, this reaction is the highest contributor to GA formation, as previously seen in Figure 11a. According to this analysis, the formation of GA directly from cellulose chain ends and mid-chain groups via retro-Diels–Alder reactions is minor. It is plausible that some of these reactions get activated at higher temperatures and are currently underpredicted by the model. Therefore, revisiting

https://doi.org/10.1021/acsengineeringau.2c00006
ACS Eng. Au 2022, 2, 320–332

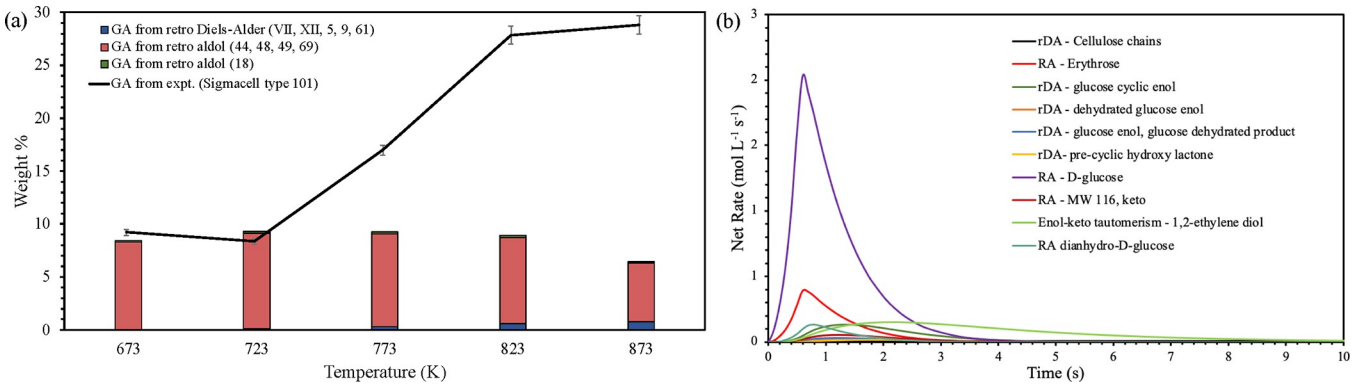

Figure 11. (a) Glycolaldehyde yields of SigmaCell Type 101 (line) and the model showing contributions from various reactions (blue: retro-Diels−Alder reactions VII, XII, 5, 9, and 61; red: retro-aldol reactions 44, 48, 49, and 69; green: retro-aldol reaction 18), and (b) net rate analysis of different reactions that contribute toward the formation of glycolaldehyde (T = 773 K). These reactions are represented in Schemes S2, S4, and S5 in the SI.

the retro-Diels−Alder reactions of cellulose chains is needed to predict GA yields accurately.

Based on the qualitative char analysis, it is evident that a different intermediate phase is involved during the pyrolysis of the two SigmaCell samples. With the insights obtained from experimental and modeling data, it is understood that there exist alternative pathways for the formation of LVG and GA from cellulose mid-chain groups that are not accounted for in the current model framework. Additional analysis through the kinetic model and updated theoretical calculations of the reactivity of mid-groups of cellulose may be required to have a clearer picture of the underlying chemistry. Nevertheless, this work establishes that intra- and interchain hydrogen bonding networks have a remarkable influence on the cellulose decomposition pathways and primarily affect the LVG yields.

4. CONCLUSIONS

Pyrolysis of celluloses with different average particle sizes (17, 35, and 57 μm) and crystallinity indices (45 and 90%) was studied using a micropyrolyzer unit combined with a GC × GC-FID/TOF-MS and a customized GC-TCD. About 60 product species, including water, were identified and quantified using comprehensive analytics. For the first time, water produced by dehydration reactions was measured directly instead of being estimated based on related product species. The levoglucosan yields from SigmaCell Types 20 and 50 are consistent with those reported in the literature. For highly purified fibers of SigmaCell Type 101, the decrease in the LVG levels was offset by increased fragmentation products, water, and GA.

Experimental observations of this study suggested that crystallinity significantly impacts the initial thermal decomposition reactions relative to the effect of particle size. Moreover, the physical state of char indicated that the Type 50 sample pyrolyzed through an intermediate molten phase, while Type 101 reacted in the solid phase. Increased amorphous sites in cellulose could promote mid-chain reactions, and their corresponding activation energies seemed to be strongly affected. Total LVG yields dropped to ∼20 wt % as opposed to the typical values of ∼60 wt %. Net rate analysis of GA formation indicated that the retro-aldol reaction of D-glucose is the most dominant pathway in the current model. However, more investigation into retro-Diels−Alder reactions of cellulose chains needs to be done to better to understand the mechanisms of GA formation during cellulose pyrolysis. The simulated yields with the modified kinetic parameters for mid-chain dehydration and fragmentation reactions showed a reasonably good agreement with the experimental data of Type 101 for water and total LMWP yields. These observations support the hypothesis that mid-chain reactions are dominating for amorphous cellulose. At the same time, for crystalline samples, decomposition occurs mainly via end-chain reactions due to the stabilizing effect of the closely packed chain structure on the glucose moiety of cellulose crystals.

■ ASSOCIATED CONTENT

Supporting Information

The Supporting Information is available free of charge at https://pubs.acs.org/doi/10.1021/acsengineeringau.2c00006.

GC × GC temperature program; temperature profiles along the reactor; reaction schemes for cellulose decomposition; char formation and LMWP formation from glucose intermediate; structural representation of fragmentation reactions; quantified pyrolysis vapor compositions of SigmaCell Types 50 and 101 collected at temperatures of 673-873 K (PDF)

■ AUTHOR INFORMATION

Corresponding Author

Kevin M. Van Geem − *Laboratory for Chemical Technology, Ghent University, Ghent 9052, Belgium;* orcid.org/0000-0003-4191-4960; Email: Kevin.VanGeem@UGent.be

Authors

Gorugantu SriBala − *Laboratory for Chemical Technology, Ghent University, Ghent 9052, Belgium; Department of Chemical and Biological Engineering, Northwestern University, Evanston, Illinois 60208, United States;* orcid.org/0000-0001-8624-2251

Diana C. Vargas − *Laboratory for Chemical Technology, Ghent University, Ghent 9052, Belgium*

Pavlo Kostetskyy − *Department of Chemical and Biological Engineering, Northwestern University, Evanston, Illinois 60208, United States;* orcid.org/0000-0003-2796-0362

Ruben Van de Vijver − *Laboratory for Chemical Technology, Ghent University, Ghent 9052, Belgium;* orcid.org/0000-0003-0605-8513

https://doi.org/10.1021/acsengineeringau.2c00006
ACS Eng. Au 2022, 2, 320−332

Linda J. Broadbelt − *Department of Chemical and Biological Engineering, Northwestern University, Evanston, Illinois 60208, United States;* orcid.org/0000-0003-4253-592X

Guy B. Marin − *Laboratory for Chemical Technology, Ghent University, Ghent 9052, Belgium;* orcid.org/0000-0002-6733-1213

Complete contact information is available at: https://pubs.acs.org/10.1021/acsengineeringau.2c00006

Notes

The authors declare no competing financial interest.

■ ACKNOWLEDGMENTS

The authors thank Dr. Hilde Poelman for her assistance with cellulose sample characterization (XRD and SEM). The research leading to these results has received funding from the European Research Council under the European Union's Seventh Framework Programme (FP7/2007-2013)/ERC grant agreement no. 290793, the "Long Term Structural Methusalem Funding by the Flemish Government", and "Bioleum" supported by the Institute for Promotion of Innovation through Science and Technology in Flanders (IWT). G.S. acknowledges a CWO travel grant received from Ghent University that facilitated the collaboration with Northwestern University. D.C.V. acknowledges support from the Belgian Development Cooperation through VLIR-UOS. The research leading to these results has also received funding from the European Research Council under the European Union's Horizon 2020 research and innovation programme/ERC grant agreement no. 818607.

■ REFERENCES

(1) SriBala, G.; Carstensen, H. H.; Van Geem, K. M.; Marin, G. B. Measuring biomass fast pyrolysis kinetics: State of the art. *Wiley Interdiscip. Rev.: Energy Environ.* **2019**, *8*, No. e326.

(2) Nishiyama, Y.; Langan, P.; Chanzy, H. Crystal Structure and Hydrogen-Bonding System in Cellulose Iβ from Synchrotron X-ray and Neutron Fiber Diffraction. *J. Am. Chem. Soc.* **2002**, *124*, 9074−9082.

(3) Nishiyama, Y.; Sugiyama, J.; Chanzy, H.; Langan, P. Crystal Structure and Hydrogen Bonding System in Cellulose Iα from Synchrotron X-ray and Neutron Fiber Diffraction. *J. Am. Chem. Soc.* **2003**, *125*, 14300−14306.

(4) Patwardhan, P. R.; Satrio, J. A.; Brown, R. C.; Shanks, B. H. Product distribution from fast pyrolysis of glucose-based carbohydrates. *J. Anal. Appl. Pyrolysis* **2009**, *86*, 323−330.

(5) Patwardhan, P. R.; Dalluge, D. L.; Shanks, B. H.; Brown, R. C. Distinguishing primary and secondary reactions of cellulose pyrolysis. *Bioresour. Technol.* **2011**, *102*, 5265−5269.

(6) Zhou, X.; Nolte, M. W.; Mayes, H. B.; Shanks, B. H.; Broadbelt, L. J. Experimental and Mechanistic Modeling of Fast Pyrolysis of Neat Glucose-Based Carbohydrates. 1. Experiments and Development of a Detailed Mechanistic Model. *Ind. Eng. Chem. Res.* **2014**, *53*, 13274−13289.

(7) Kobayashi, Y.; Horie, Y.; Honjo, K.; Uemura, T.; Kitagawa, S. The controlled synthesis of polyglucose in one-dimensional coordination nanochannels. *Chem. Commun.* **2016**, *52*, 5156−5159.

(8) Vitasari, C. R.; Meindersma, G. W.; de Haan, A. B. Laboratory scale conceptual process development for the isolation of renewable glycolaldehyde from pyrolysis oil to produce fermentation feedstock. *Green Chem.* **2012**, *14*, 321−325.

(9) Luebben, S. D.; Raebiger, J. W., A Novel Renewable Thermoplastic Polyacetal by Polymerization of Glycolaldehyde Dimer, a Major Product of the Fast Pyrolysis of Cellulosic Feedstock. In *Green Polymer Chemistry: Biobased Materials and Biocatalysis*, American Chemical Society: 2015; Vol. *1192*, pp. 305−328, DOI: 10.1021/bk-2015-1192.ch019.

(10) Pang, J.; Zheng, M.; Sun, R.; Wang, A.; Wang, X.; Zhang, T. Synthesis of ethylene glycol and terephthalic acid from biomass for producing PET. *Green Chem.* **2016**, *18*, 342−359.

(11) Mettler, M. S.; Mushrif, S. H.; Paulsen, A. D.; Javadekar, A. D.; Vlachos, D. G.; Dauenhauer, P. J. Revealing pyrolysis chemistry for biofuels production: Conversion of cellulose to furans and small oxygenates. *Energy Environ. Sci.* **2012**, *5*, 5414−5424.

(12) Zhou, X.; Nolte, M. W.; Shanks, B. H.; Broadbelt, L. J. Experimental and mechanistic modeling of fast pyrolysis of neat glucose-based carbohydrates. 2. Validation and evaluation of the mechanistic model. *Ind. Eng. Chem. Res.* **2014**, *53*, 13290−13301.

(13) Maduskar, S.; Facas, G. G.; Papageorgiou, C.; Williams, C. L.; Dauenhauer, P. J. Five Rules for Measuring Biomass Pyrolysis Rates: Pulse-Heated Analysis of Solid Reaction Kinetics of Lignocellulosic Biomass. *ACS Sustainable Chem. Eng.* **2018**, *6*, 1387−1399.

(14) Proano-Aviles, J.; Lindstrom, J. K.; Johnston, P. A.; Brown, R. C. Heat and Mass Transfer Effects in a Furnace-Based Micro-pyrolyzer. *Energy Technol.* **2017**, *5*, 189−195.

(15) Zhang, J.; Nolte, M. W.; Shanks, B. H. Investigation of primary reactions and secondary effects from the pyrolysis of different celluloses. *ACS Sustainable Chem. Eng.* **2014**, *2*, 2820−2830.

(16) Maduskar, S.; Maliekkal, V.; Neurock, M.; Dauenhauer, P. J. On the yield of levoglucosan from cellulose pyrolysis. *ACS Sustainable Chem. Eng.* **2018**, *6*, 7017−7025.

(17) Patwardhan, P. R.; Satrio, J. A.; Brown, R. C.; Shanks, B. H. Influence of inorganic salts on the primary pyrolysis products of cellulose. *Bioresour. Technol.* **2010**, *101*, 4646−4655.

(18) Zhou, X.; Mayes, H. B.; Broadbelt, L. J.; Nolte, M. W.; Shanks, B. H. Fast pyrolysis of glucose-based carbohydrates with added NaCl part 1: Experiments and development of a mechanistic model. *AIChE J.* **2016**, *62*, 766−777.

(19) Arora, J. S.; Chew, J. W.; Mushrif, S. H. Influence of alkali and alkaline-earth metals on the cleavage of glycosidic bond in biomass pyrolysis: a DFT study using cellobiose as a model compound. *J. Phys. Chem. A* **2018**, *122*, 7646−7658.

(20) Arora, J. S.; Ansari, K. B.; Chew, J. W.; Dauenhauer, P. J.; Mushrif, S. H. Unravelling the catalytic influence of naturally occurring salts on biomass pyrolysis chemistry using glucose as a model compound: a combined experimental and DFT study. *Catal. Sci. Technol.* **2019**, *9*, 3504−3524.

(21) SriBala, G.; Vinu, R. Unified Kinetic Model for Cellulose Deconstruction via Acid Hydrolysis. *Ind. Eng. Chem. Res.* **2014**, *53*, 8714−8725.

(22) SriBala, G.; Chennuru, R.; Mahapatra, S.; Vinu, R. Effect of alkaline ultrasonic pretreatment on crystalline morphology and enzymatic hydrolysis of cellulose. *Cellulose* **2016**, *23*, 1725−1740.

(23) Broido, A.; Javier-Son, A. C.; Ouano, A. C.; Barrall, E. M. Molecular weight decrease in the early pyrolysis of crystalline and amorphous cellulose. *J. Appl. Polym. Sci.* **1973**, *17*, 3627−3635.

(24) Katō, K.; Komorita, H. Pyrolysis of Cellulose: Part IV. Effect of Crystallinity of Cellulose on the Formation of the Volatile Compounds. *Agric. Biol. Chem.* **1968**, *32*, 21−26.

(25) Schultz, T. P.; McGinnis, G. D.; Nicholas, D. D. Effect of crystallinity and additives on the thermal degradation of cellulose. *ACS Publications* **1990**, 335−360.

(26) Gurgel, L. V. A.; Marabezi, K.; Ramos, L. A.; da Silva Curvelo, A. A. Characterization of depolymerized residues from extremely low acid hydrolysis (ELA) of sugarcane bagasse cellulose: Effects of degree of polymerization, crystallinity and crystallite size on thermal decomposition. *Ind. Crops Prod.* **2012**, *36*, 560−571.

(27) Mukarakate, C.; Mittal, A.; Ciesielski, P. N.; Budhi, S.; Thompson, L.; Iisa, K.; Nimlos, M. R.; Donohoe, B. S. Influence of Crystal Allomorph and Crystallinity on the Products and Behavior of Cellulose during Fast Pyrolysis. *ACS Sustainable Chem. Eng.* **2016**, *4*, 4662−4674.

(28) Poletto, M.; Pistor, V.; Zeni, M.; Zattera, A. J. Crystalline properties and decomposition kinetics of cellulose fibers in wood pulp

obtained by two pulping processes. *Polym. Degrad. Stab.* **2011**, *96*, 679−685.
(29) Kim, U.-J.; Eom, S. H.; Wada, M. Thermal decomposition of native cellulose: influence on crystallite size. *Polym. Degrad. Stab.* **2010**, *95*, 778−781.
(30) Wang, Z.; McDonald, A. G.; Westerhof, R. J. M.; Kersten, S. R. A.; Cuba-Torres, C. M.; Ha, S.; Pecha, B.; Garcia-Perez, M. Effect of cellulose crystallinity on the formation of a liquid intermediate and on product distribution during pyrolysis. *J. Anal. Appl. Pyrolysis* **2013**, *100*, 56−66.
(31) SriBala, G.; Van de Vijver, R.; Li, L.; Dogu, O.; Marin, G. B.; Van Geem, K. M. On the primary thermal decomposition pathways of hydroxycinnamic acids. *Proc. Combust. Inst.* **2021**, *38*, 4207−4214.
(32) Pyl, S. P.; Schietekat, C. M.; Van Geem, K. M.; Reyniers, M.-F.; Vercammen, J.; Beens, J.; Marin, G. B. Rapeseed oil methyl ester pyrolysis: On-line product analysis using comprehensive two-dimensional gas chromatography. *J. Chromatogr. A* **2011**, *1218*, 3217−3223.
(33) Kostetskyy, P.; Coile, M. W.; Terrian, J. M.; Collins, J. W.; Martin, K. J.; Brazdil, J. F.; Broadbelt, L. J. Selective production of glycolaldehyde via hydrothermal pyrolysis of glucose: Experiments and microkinetic modeling. *J. Anal. Appl. Pyrolysis* **2020**, *149*, No. 104846.
(34) Stewart, W. E.; Caracotsios, M.; Sorenson, J. P., *DDASAC Software Package Documentation*. Department of Chemical Engineering, University of Wisconsin: Madison, 1994.
(35) Innerlohinger, J.; Kraft, G.; Weber, H.; Harms, H., Cellulose powder and processes for its production. U.S. Patent No. 9,163,095. Washington, DC: U.S. Patent and Trademark Office, 2015.
(36) Deneyer, A.; Ennaert, T.; Cavents, G.; Dijkmans, J.; Vanneste, J.; Courtin, C. M.; Dusselier, M.; Sels, B. F. Compositional and structural feedstock requirements of a liquid phase cellulose-to-naphtha process in a carbon-and hydrogen-neutral biorefinery context. *Green Chem.* **2016**, *18*, 5594−5606.
(37) Krumm, C.; Pfaendtner, J.; Dauenhauer, P. J. Millisecond pulsed films unify the mechanisms of cellulose fragmentation. *Chem. Mater.* **2016**, *28*, 3108−3114.
(38) Teixeira, A. R.; Mooney, K. G.; Kruger, J. S.; Williams, C. L.; Suszynski, W. J.; Schmidt, L. D.; Schmidt, D. P.; Dauenhauer, P. J. Aerosol generation by reactive boiling ejection of molten cellulose. *Energy Environ. Sci.* **2011**, *4*, 4306−4321.
(39) Gong, X.; Yu, Y.; Gao, X.; Qiao, Y.; Xu, M.; Wu, H. Formation of Anhydro-sugars in the Primary Volatiles and Solid Residues from Cellulose Fast Pyrolysis in a Wire-Mesh Reactor. *Energy Fuels* **2014**, *28*, 5204−5211.
(40) Cao, J.; Yu, Y.; Wu, H. Contributions of Thermal Ejection and Evaporation to the Formation of Condensable Volatiles during Cellulose Pyrolysis. *Energy Fuels* **2022**, *36*, 1939−1947.
(41) Hosoya, T.; Sakaki, S. Levoglucosan formation from crystalline cellulose: importance of a hydrogen bonding network in the reaction. *ChemSusChem* **2013**, *6*, 2356−2368.
(42) Agarwal, V.; Huber, G. W.; Conner, W. C., Jr.; Auerbach, S. M. Simulating infrared spectra and hydrogen bonding in cellulose Iβ at elevated temperatures. *J. Chem. Phys.* **2011**, *135*, 10B605.
(43) Padmanathan, A. M. D.; Mushrif, S. H. Pyrolytic activation of cellulose: energetics and condensed phase effects. *React. Chem. Eng.* **2022**, DOI: 10.1039/D1RE00492A.

https://doi.org/10.1021/acsengineeringau.2c00006
ACS Eng. Au 2022, 2, 320−332